JOURNAL OF GEOPHYSICAL RESEARCH, VOL. 113, C08031, doi:10.1029/2008JC004726, 2008

Click Here for Full Article

Shoaling of nonlinear internal waves in Massachusetts Bay

A. Scotti,[1] R. C. Beardsley,[2] B. Butman,[3] and J. Pineda[4]

Received 8 January 2008; revised 19 March 2008; accepted 2 April 2008; published 19 August 2008.

[1] The shoaling of the nonlinear internal tide in Massachusetts Bay is studied with a fully nonlinear and nonhydrostatic model. The results are compared with current and temperature observations obtained during the August 1998 Massachusetts Bay Internal Wave Experiment and observations from a shorter experiment which took place in September 2001. The model shows how the approaching nonlinear undular bore interacts strongly with a shoaling bottom, offshore of where KdV theory predicts polarity switching should occur. It is shown that the shoaling process is dominated by nonlinearity, and the model results are interpreted with the aid of a two-layer nonlinear but hydrostatic model. After interacting with the shoaling bottom, the undular bore emerges on the shallow shelf inshore of the 30-m isobath as a nonlinear internal tide with a range of possible shapes, all of which are found in the available observational record.

Citation: Scotti, A., R. C. Beardsley, B. Butman, and J. Pineda (2008), Shoaling of nonlinear internal waves in Massachusetts Bay, *J. Geophys. Res.*, *113*, C08031, doi:10.1029/2008JC004726.

1. Introduction

[2] While modeling and observations of propagating nonlinear internal waves (NLIWs) in the ocean (both in shallow and deep seas) form by now a well established body of literature (see, e.g., the recent reviews by *Apel et al.* [2007] and *Helfrich and Melville* [2006], and references therein) the interaction of NLIWs with a shoaling bottom remains a problem of considerable interest in coastal oceanography. According to weakly nonlinear theory, the polarity of a steady NLIW is always such that the wave thickens the thinner of the two layers separated by the pycnocline. Therefore when the pycnocline is closer to the surface, nonlinear waves can only propagate as waves of depression, and vice versa when the pycnocline sits near the bottom, as waves of elevation. A particularly interesting case is when, due to a shoaling bottom, a given isobath divides the domain in two regions, offshore (shoreward) of which only waves of depression (elevation) are possible. At the critical isobath, the coefficient of the quadratic term in the weakly nonlinear expansion vanishes, and higher order terms have to be included [*Grimshaw et al.*, 1999]. The main result of these higher order theories is that the incoming wave of depression switches polarity at the critical depth. In the process, some energy can be radiated offshore to ensure conservation of mass.

[3] Weakly nonlinear theories are fundamental in framing the problem. However, field evidence shows that most waves of depression found in nature are highly nonlinear [*Stanton and Ostrovsky*, 1998; *Ramp et al.*, 2004], and it is reasonable that any transition to waves of elevation should retain the degree of nonlinearity of the parent waves. Also, highly nonlinear waves may "feel" the bottom much sooner than weakly nonlinear theories predict. This is particularly important in Massachusetts Bay since the seasonal pycnocline is shallow.

[4] Because of the proximity with the surface, waves of depression have a clear signature that can be detected via remote sensing [*Apel et al.*, 1995], their existence is well documented [*Jackson*, 2004], and their properties known. Wave-like features in SAR images have been occasionally ascribed to waves of elevation [*Liu et al.*, 1998], but without a direct comparison to in situ data. Thus until recently, the existence of near-bottom waves of elevation was a matter of speculation. That changed with the publication, in the last few years, of several papers which provided the first detailed descriptions of the physical properties of waves of elevation observed in the field [*Klymak and Moum*, 2003; *Scotti and Pineda*, 2004; *Bourgault et al.*, 2007]. These studies found strong evidence of trapped cores within the leading waves, which is surprising, given that trapped cores are rarely found in waves of depression. In the study by *Scotti and Pineda* [2004], the origin of the waves was traced to waves of depression that were found propagating further offshore, but no detailed explanation was given of the link. *Bourgault et al.* [2007] modeled the runup of NLIWs in the St. Lawrence Estuary, showing how NLIWs of elevation in the form of boluses can form.

[5] Before the publication of these papers, laboratory [*Helfrich and Melville*, 1986; *Helfrich*, 1992; *Kao et al.*, 1985] and, more recently, numerical experiments [*Vlasenko and Hutter*, 2002; *Legg and Adcroft*, 2003; *Vlasenko et al.*, 2005a; *Venayagamoorthy and Fringer*, 2006] considered the problem of waves of depression approaching a shoaling bottom. In the work of *Vlasenko et al.* [2005a] the interac-

[1]Department of Marine Sciences, University of North Carolina, Chapel Hill, North Carolina, USA.
[2]Department of Physical Oceanography, Woods Hole Oceanographic Institution, Woods Hole, Massachusetts, USA.
[3]U.S. Geological Survey, Woods Hole Science Center, Woods Hole, Massachusetts, USA.
[4]Biology Department, Woods Hole Oceanographic Institution, Woods Hole, Massachusetts, USA.

Copyright 2008 by the American Geophysical Union.
0148-0227/08/2008JC004726$09.00

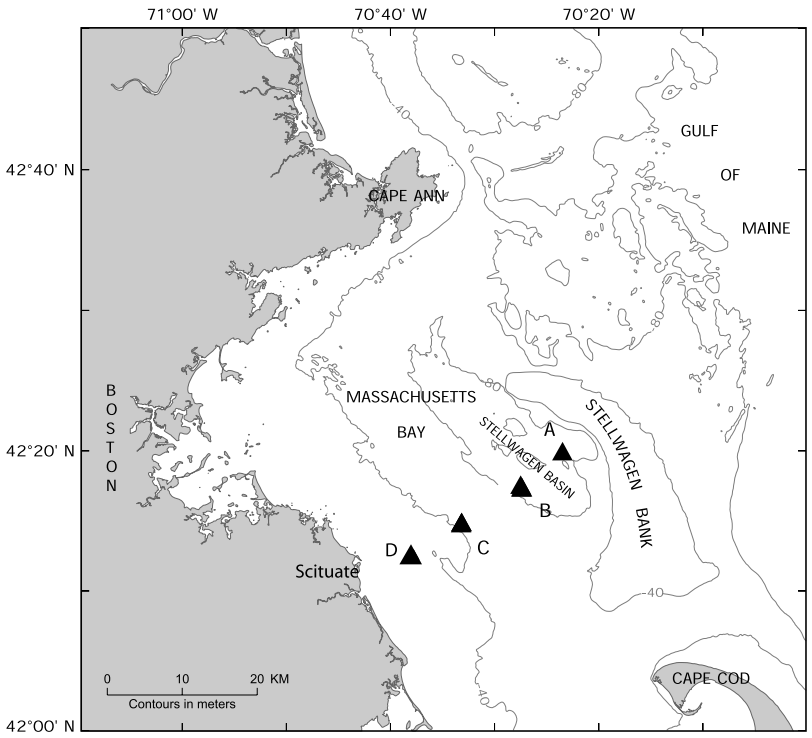

Figure 1. Map of Massachusetts Bay showing the mooring locations. A, B, and C were occupied during the 1998 Massachusetts Bay Internal Waves Experiment. A location slightly inshore of C was reoccupied in September 2001 for a week together with mooring D.

tion is adiabatic, and no switch in polarity is considered. In the other studies, the shared result is that the shoaling/polarity switching process can be highly nonlinear. However, these approaches were hampered by a number of issues, chiefly the scale mismatch, and the lack of real turbulence. Typically, the topographic scale-to-wavelength ratio in the field exceeds 10, while in lab and numerical experiments it is close to one. This scale compression affects other parameters as well. For example, by *Venayagamoorthy and Fringer* [2006], the frequency of the incoming wave was more than half the Brünt-Väisälä (B-V) frequency. As a consequence, no higher-harmonics could propagate as free waves. *Dauxois and Young* [1999] showed that when scattering from a near-critical slope, higher-order harmonics are important in carrying away some of the energy that otherwise would be trapped in the near-bottom region. Also, at lab scales the Reynolds numbers that can be achieved are modest. Numerical models, on the other hand, can reach large nominal values of the Reynolds number, but cannot contain any realistic turbulence due to scale limitation, and at best have to resort to ad hoc parameterization of the turbulent stresses [*Legg and Adcroft*, 2003]. However, these issues may not be critical, if we can a posteriori verify the prediction of inviscid models with field data (or lab data, if of high enough Reynolds numbers).

[6] In this paper, we compare results from a numerical model with data from two experiments: the 1998 joint USGS-WHOI Massachusetts Bay Internal Wave Experiment (MBIWE98) and a shorter, 1-week long, experiment conducted in the same area in September 2001. The first experiment was conducted primarily to asses the role played by NLIWs routinely observed in the area in resuspending sediments, but also provided high quality water column measurements of waves during generation, propagation and shoaling (locations A, B and C in Figure 1). Details of the experiment is discussed by *Butman et al.* [2004a, 2006]. The second experiment focused on the interaction of plankton with propagating NLIWs. Moorings were deployed on the slope and shelf section (locations C and D in Figure 1) to characterize the evolution of NLIWs as they move from the deep to the shallow side of the Bay [*Scotti and Pineda*, 2004]. The appeal of Massachusetts Bay for the study of NLIWs is that the generation-propagation-shoaling process occurs within a distance less than 30 km long. Therefore a single domain (albeit still two-dimensional) can be used to study the entire process. Also, the slope of the shoaling seafloor west of Stellwagen Basin is mild (about 0.5°). Since the amplitude of the incoming waves is such that the ratio $a/(D - h_p) \leq 1$ (where a is the displacement of the leading wave, D the local depth and h_p the depth of the undisturbed pycnocline), the shoaling waves do not collapse as they would if the slope where steeper [*Vlasenko et al.*, 2005b, p. 239].

[7] The model is fully nonlinear and nonhydrostatic, and allows the simulation of NLIWs from generation over Stellwagen Bank to shoaling along a transect extending from Stellwagen Bank westward to just offshore of Scituate, Massachusetts (Figure 1). In a companion paper [*Scotti et al.*, 2007], herein referred as SBB1, we described the model in detail, discussed the mechanism of generation of NLIWs in the area, and how they evolve in the Bay. Here we focus on the processes that occur when the waves approach the western shallow side of the Bay. Both model and field data will be considered. For completeness, we summarize the

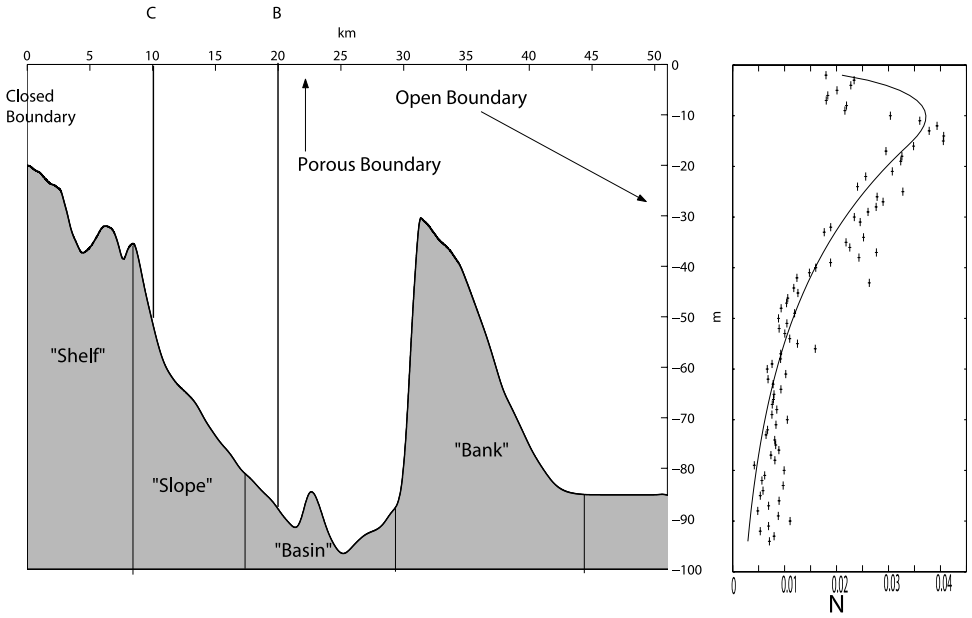

Figure 2. Schematic of the physical domain employed in the present study (left) and observed versus modeled stratification (right). The bottom depth follows the topography along the line connecting the moorings A through D in Figure 1 up to $x = 45$ km, after which the depth is kept constant. Also indicated are the four regions (bank, basin, slope, and shelf) used to characterize the different regimes during the presentation of the results. The thick vertical lines marked B and C show the locations of the homonymous MBIWE98 moorings. On the right side, the observed (crosses) stratification is plotted together with the stratification (solid line and standard case) used in the Euler model.

findings of SBB1 and give a brief description of the model below.

[8] The process of generation begins when the ebbing barotropic tidal flow becomes supercritical over Stellwagen Bank. A surface-trapped pool of relatively stagnant water forms just downstream of the Bank edge. As the tide slacks, the pool is released, akin to a lock-exchange problem. Initially, the leading edge of the disturbance becomes less steep, as it leaves the crest of the Bank and moves westward into deeper water. The wavefront steepens only when it reaches the deep section of the basin west of the Bank. Up to this point, the model shows that the process is mainly controlled by nonlinearity. Once steep enough, dispersive effects become important, and high-frequency nonlinear waves begin to appear near the leading edge, as the disturbance evolves into an undular bore. The amplitude of the undular bore is such that the weakly nonlinear assumption is violated under the majority of forcing and stratification conditions observed. As a consequence, the undular bore seldom appears to conform to the dnoidal solution expected in this case from weakly nonlinear theory [*Apel*, 2003]. Having discussed generation and propagation in SBB1, here we focus on the fate of the undular bore as it approaches the shoaling area west of the basin.

2. Numerical Model

[9] To study the evolution of NLIWs as they approach the shallow end of Massachusetts Bay we use the same fully nonlinear and nonhydrostatic numerical model described in SBB1, to which the reader is referred for details. The model solves the Euler equations in a two-dimensional channel with variable bottom geometry, simulating the topography measured along the track connecting the moorings deployed during MBIWE98 (Figure 2). The shoreward (west) side of the channel is closed, while it is open to the east to the incoming tidal flow. The original conservation equations are recast in streamwise-vorticity form and solved using a fully dealiased pseudospectral method. The flow is forced by the barotropic tide, which is applied so that the horizontal component of the barotropic flow goes to zero as the shore is approached. The density is written as the sum of a background component, dependent only on depth, plus a perturbation. The horizontal resolution is 1/10 of the local depth, and 33 levels are used in the vertical. For further details on the discretization, and on the linear and nondispersive (hydrostatic) limit of the model, the reader is referred to SBB1.

2.1. Stratification, Forcing and Initial Conditions

[10] To model the response of the system to changes in the mean stratification in the basin, we consider three background density profiles of the kind

$$\overline{\rho} = \begin{cases} a\left(b - e^{z/c+0.3125}\right) & \text{if } z/c \le -1, \\ a\left(b - e^{z/c+0.3125} + d(z/c+1)^f\right) & \text{if } -1 \le z/c \le 0, \end{cases} \tag{1}$$

[11] The parameters employed are listed in Table 1. The maximum value of the B-V frequency is constant in all cases (0.037 s^{-1}), but the location of the pycnocline changes from 6 (Shallow case) to 10 (Standard case) to 16.5 m (Deep case). The Brunt-Väisälä frequency versus depth profile for the Standard case is shown in Figure 2

Table 1. Parameters Used for Computing the Stratification Profile in the Three Cases Considered Equation (1)

	A (σ)	B	C (m)	D	F	Pycnocline Depth (m)
Standard	3.55	7.17	16	0.37	3.6	10
Shallow	2.25	11.33	10	0.37	3.6	6
Deep	5.833	4.385	24	0.40	3	16.5

together with values measured during MBIWE98. The profile shows clearly the existence of the strong seasonal thermocline that provides the waveguide for NLIWs, which justifies the two-layer assumption in the simplified models considered in section 3.5 below.

[12] The waves are forced by prescribing the barotropic tide with period of 12.42 h. To consider the different tidal regimes (neap, standard, spring), we use three different values for the amplitude of the tide in midbasin (Table 2).

3. Shoaling of NLIWs

3.1. Observational Data

[13] The 50-m isobath is an area of rapid across-shore variation in bottom surficial sediment texture [*Butman et al.*, 2004b]. Inshore of this isobath, the bottom is mainly covered with gravel and sand, while offshore mud dominates. The transition occurs over a few hundred meters [see *Butman et al.*, 2006, Figures 3 and 4]. Analysis of Synthetic Aperture Radar images in the area did not reveal NLIWs inshore of the 40-m isobath [*Trask and Briscoe*, 1983]. Thus both geological and remote-sensing evidence point to this area as a good candidate location for observing shoaling of NLIWs. This location (C in Figure 1) was occupied during MBIWE98 with surface and subsurface moorings which included an upward-looking ADCP and several temperature and conductivity sensors spanning the water column [*Butman et al.*, 2006]. In September 2001 a mooring with 11 SBE39 temperature sensors was deployed slightly inshore (water depth 45 m). A second mooring was deployed further inshore, at the 25-m isobath (D in Figure 1), featuring five temperature sensors and an upward looking ADCP [*Scotti and Pineda*, 2004]. In this second experiment, data were collected over a week-long period.

[14] During MBIWE98, until 18 August the NLIWs observed at C were of the undular bore type (Figure 3a), not dissimilar from the ones observed in the middle of Stellwagen Basin (SBB1). High-frequency oscillations were confined to the upper third of the water column, with isopycnals displacements of the order of 20 m (SBB1). The leading edge of the undular bore arrived regularly 10.18 ± 1.15 h after low tide (as measured at B).

[15] After 18 August instead of undular bores, we consistently observed energetic events, which we called Bottom Collision Events (BCEs). These events are characterized by three phases: (1) a deepening of the pycnocline, ending very near the bottom, followed by (2) a period during which the pycnocline remained close to the bottom, after which (3) it quickly returned close to its equilibrium condition, often accompanied by mode-1 and -2 high-frequency oscillations (Figure 3b). During the period of maximum isopycnals downward displacement, near-bottom currents exceeded 60 cm/s in the offshore direction, over twice as large as the value measured during the passage of normal undular bores. Also, at mid depth, the currents switched from offshore to onshore as the event progressed (Figure 4). Unlike undular bores, these events produce large temperature variations at the bottom. The occurrence of these events did not correlate with the strength of the barotropic forcing. Instead, we found a strong threshold dependence on the depth of the pycnocline at B (Figure 5). During MBIWE98, the maximum value of the Brünt-Väisäla frequency did not vary appreciably. However, the depth of the pycnocline deepened, probably in response to a combination of synoptic forcing and seasonal warming. BCEs were observed only when the pycnocline at B was deeper than 10 m. In the 2001 experiment, during which data were collected at a slightly more inshore location and later in the season, BCEs were observed consistently during the entire period (Figures 3c–3d).

[16] Phase 2 is the most robust property of all the BCEs observed. Both the initial deepening of the thermocline (phase 1), as well as the return to its equilibrium position (phase 3) can be gradual or abrupt, and high-frequency oscillations may or may not be present. For example, during the BCE observed on 16 September 2001 (Figure 3c), the pycnocline deepened very rapidly, but the recovery occurred rather gradually, whereas on 17 September the restoration of the pycnocline was rapid, and accompanied by high frequency oscillations (Figure 3d). Despite these differences, the observational evidence shows that BCEs are a robust feature of the NLIWs observed in this area during the late summer.

3.2. Model Results

[17] In SBB1 we used the model to study how the waves were generated over Stellwagen Bank and evolved as they propagate westward across Stellwagen Basin. Generally, it was found that in the middle of Stellwagen Basin, NLIWs propagate as an undular bore of depression. Here, we start from where we left off in SBB1. In all cases, we have an undular bore approaching the shoaling area. As in SBB1, we consider the different cases separately.

3.2.1. Standard Case

[18] In the standard case, the undular bore approaches the shoaling region as a packet of about 10 waves, stretching over 2 km (Figure 6). As the bottom shoals, the trough of the leading edge becomes flat. The process further intensifies as the packet moves toward shallower water, until a situation is reached where the leading edge of the undular bore moves ahead as a rarefaction wave, accelerating the fluid below the pycnocline, which tends to align itself to the bottom. The following waves attempt to propagate into a

Table 2. Maximum Value of the Barotropic Tidal Current[a]

	Mid-Basin (m/s)	Stellwagen Bank (m/s)
Mean	0.13	0.52
Spring	0.16	0.65
Neap	0.10	0.39

[a]The values in the middle of Stellwagen Basin are based on observations at location B (Figure 1). The values over Stellwagen Bank the values are calculated assuming constant transport.

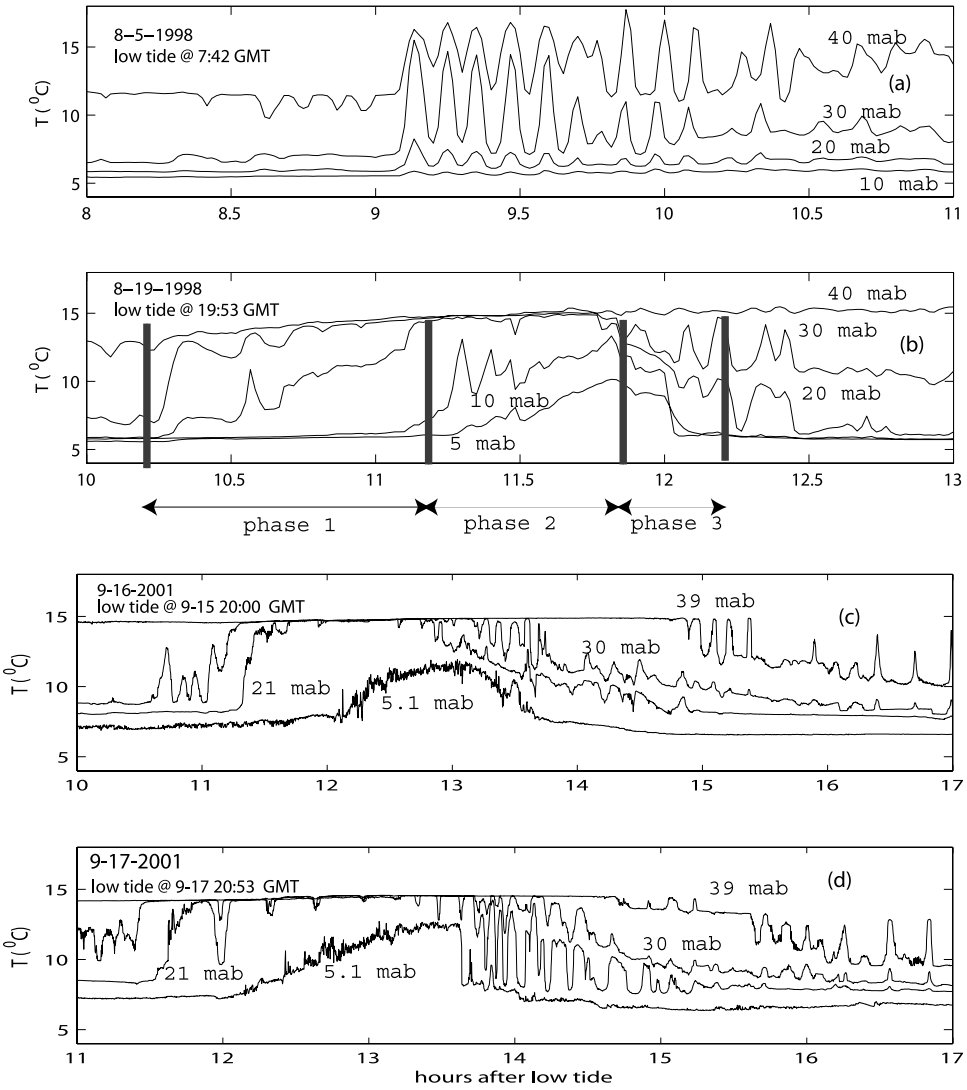

Figure 3. Examples of NLIWs observed at C (Figure 1) in the temperature record. An increase in temperature denotes downward displacement of isotherms. Figure 3a shows the passage of an undular bore, similar in shape and properties to the ones that are normally observed propagating in the deeper section of the Bay. During MBIWE98 most of the NLIWS at C were of this type. Figures 3b–3d show examples of BCEs, caused by the approaching undular bore undergoing shoaling. Figure 3b is an event recorded in 1998 during MBIWE98; the vertical lines mark the temporal boundaries of the phases identified in the main text of the article. Figures 3c–3d show events observed in September 2001. Because of postprocessing resampling, the MBIWE98 time series appear smoother.

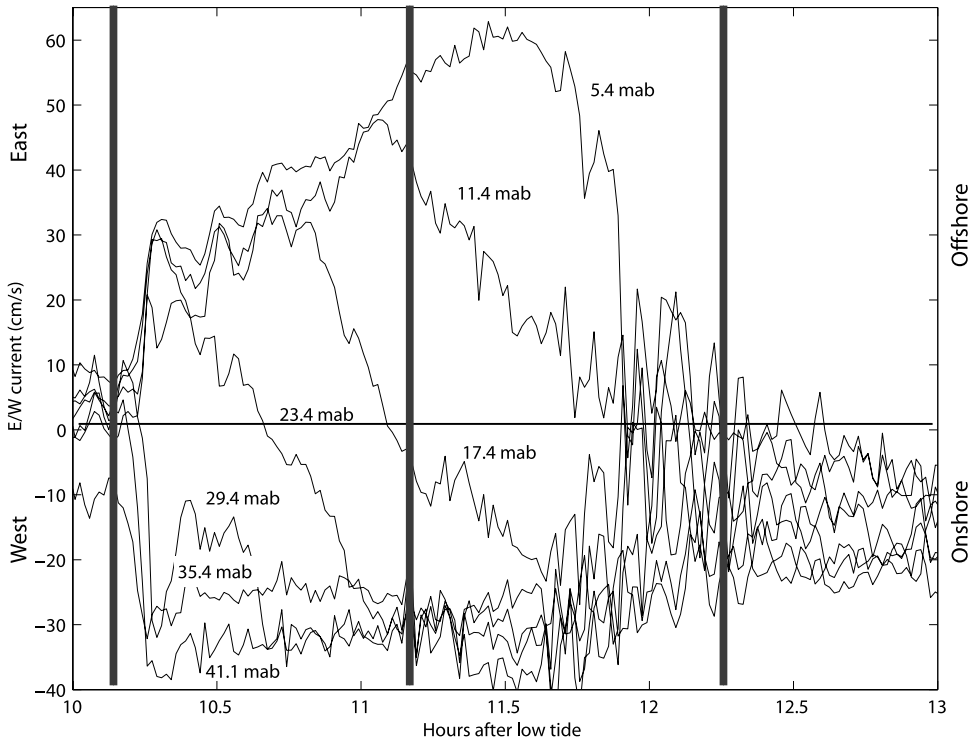

Figure 4. East–West currents at mooring C during the BCE shown in Figure 3b. Note how the offshore near-bottom current increases from 10 cm/s to over 60 cm/s, and how the currents at middepth switch from offshore to onshore, as the pycnocline is progressively lowered. Thick vertical lines as in Figure 3. Time series labeled in meters above bottom (mab).

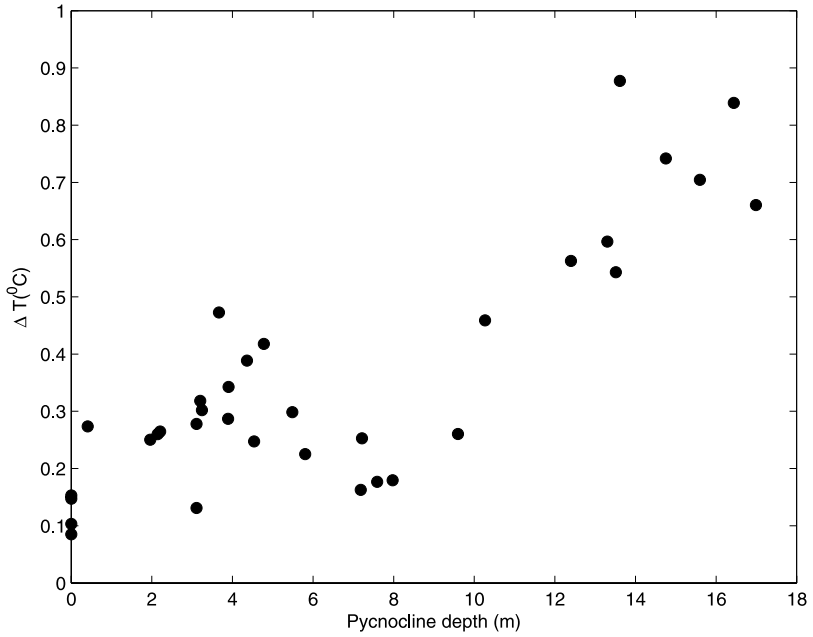

Figure 5. Scatterplot of pycnocline depth (measured at B) versus maximum bottom temperature difference during a tidal cycle observed at C. Changes in temperature in excess of 0.5°C at C, indicating the occurrence of BCEs, occur only when the pycnocline deepens below 12 m. Data from MBIWE98 experiment.

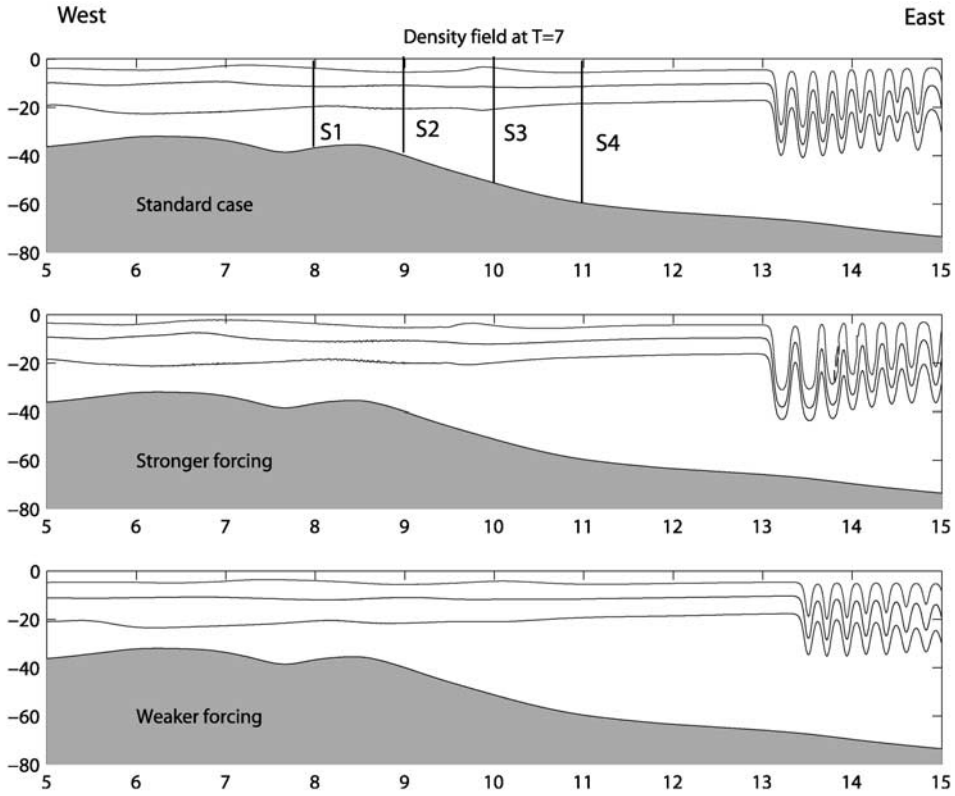

Figure 6. Density field 7 h after low tide on the western side of basin. From top to bottom, mean tide, spring tide and neap tide. The isolines contoured correspond to σ_t = 22.5, 23.5, and 24.5. Horizontal distances are in kilometers and depth in meters. The solid vertical lines show the locations of the ''virtual'' CTD stations. See Figure 10 for temperature time series at sites S1–S4.

region of strong adverse flow, become unstable and begin to break (Figures 7 and 8). During this process, the packet resembles the bellows of an accordion being squeezed, as less dense water from the shelf west of the slope flows eastward along the bottom in a narrow jet. An hydraulic jump forms near the bottom (A in Figure 8), which is advected further downstream, until the near-bottom current slacks, at which point the jump begins to propagate upslope, abruptly bringing the stratification back to its normal value. While this happens on the slope, another jump forms further up slope, bounding to the west the depression heralded by the rarefaction wave. This second jump evolves into an undular bore of elevation. The evolution of the first wave of the packet reported here resembles quite well the shoaling of single solitary waves described by *Kao et al.* [1985] (see, e.g., Figure 16 in their paper), who studied the propagation of solitary waves in a two-layer system in laboratory experiments, as well as the numerical experiments of *Vlasenko and Hutter* [2002].

3.2.2. Spring Tide

[19] The wave pattern for stronger forcing is qualitatively similar to the standard case. The amplitude of the waves in the packet is larger, hence the undular bore begins to feel the effects of the shoaling bottom earlier. Already at t = 7, we can see evidence of instabilities developing on the trailing edge of the third wave of the packet (Figure 6). By t = 7.5, the troughs of the two leading waves appear flattened, while instabilities develop on the following waves. The leading edge of the undular bore behaves essentially as in the standard case, racing forward as a rarefaction wave, accelerating the return flow below the pycnocline. Also, as in the standard case, an hydraulic jump forms very close to the bottom, initially being advected offshore, while a second jump forms in the middle of the water column, moving slowly onshore (Figure 8). In the meantime the solitary waves in the packet succumb to shearing instabilities, until we have the situation already described above, with an undular bore closing the depression formed by the rarefaction wave on the plateau, and an hydraulic jump restoring the stratification on the slope. Relative to the standard case, well defined solitary waves do not make it past $x \simeq 11$ km.

3.2.3. Neap Tide

[20] The undular bore approaching the slope during neap tide conditions differs from the cases considered above in that the amplitude is smaller, and the oscillations smoothly decay away from the leading edge, forming a long packet. Also, the effects of the shoaling bottom are not felt until the plateau is almost reached, around $x \simeq 9$ km. At this point, the packet follows a similar script. The leading edge moves forward as a rarefaction wave. The wavelength of the following waves shrink until they become unstable. As before, an hydraulic jump forms near the bottom, restoring the equilibrium stratification. On the shelf, however, the formation of the second jump is not observed.

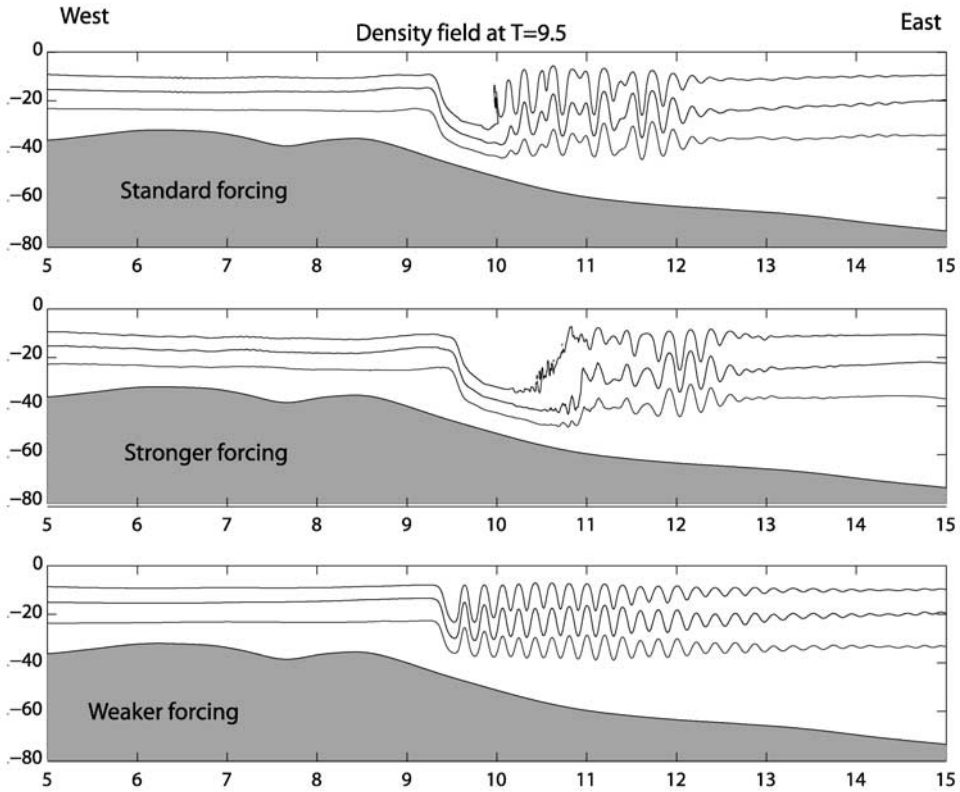

Figure 7. Density field 9.5 h after low tide on the western side of basin. From top to bottom, mean tide, spring tide and neap tide. Isolines as in Figure 6.

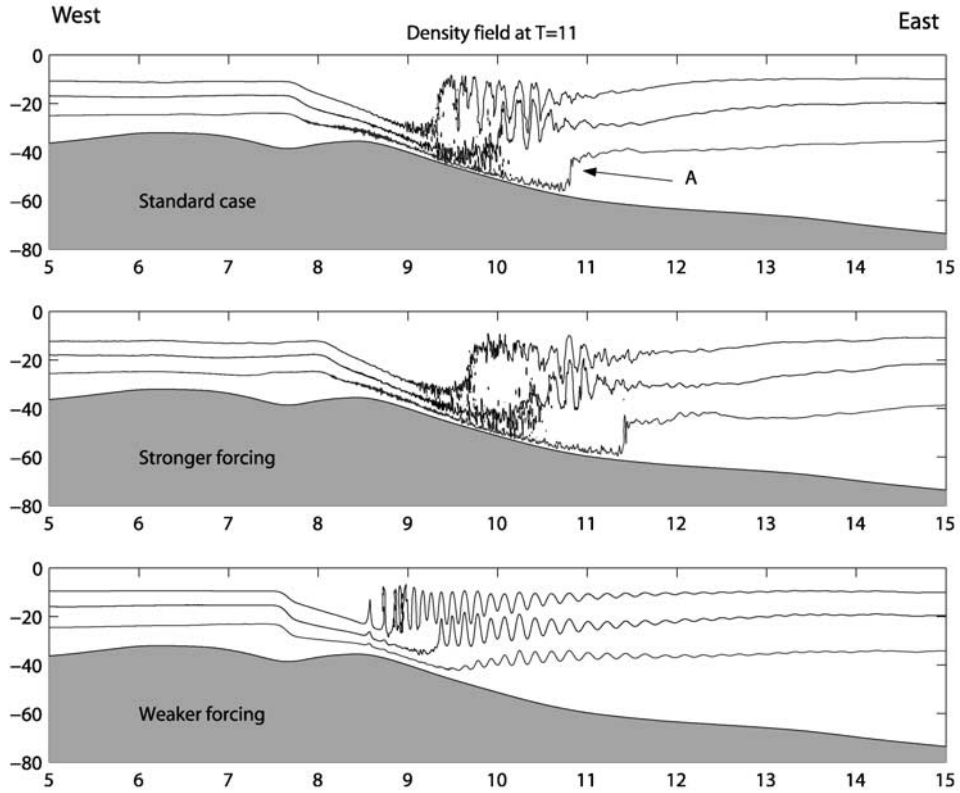

Figure 8. Density field 11 h after low tide on the western side of basin. From top to bottom, mean tide, spring tide and neap tide. Isolines as in Figure 6.

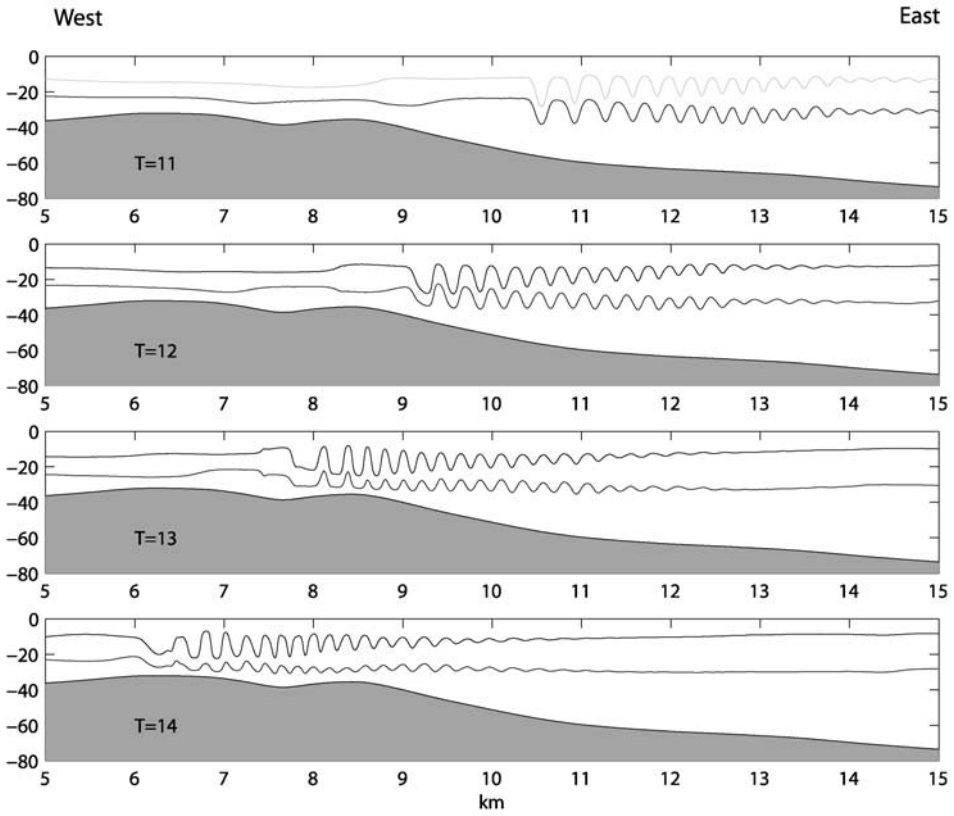

Figure 9. Shoaling of the undular bore propagating over the shallow pycnocline. The isolines contoured are for σ_t = 23 and 24. Horizontal distances are in kilometers and depth in meters.

3.2.4. Shallower Pycnocline

[21] Due to the lower propagation speed, the undular bore arrives to the shoaling region with considerable delay relative to the standard case. This means that the disturbance approaches the upper portion of the slope with the tide has turned and is flowing in the direction of propagation of the wave (inshore), as opposed to against it as in the cases considered above. As discussed in SBB1, the undular bore settles in the middle of Stellwagen Basin in a state characterized by a series of oscillations smoothly diminishing in amplitude from front to back, with more and more oscillations adding to the packet as time goes on. The amplitude of the first oscillation decreases from 25 m at t = 10, when the packet is at the beginning of the ramp leading to the 40-m isobath, to about 15 m at the 40 m isobath. Unlike the cases considered above, the packet transit over the upper portion of the slope and over the plateau is rather uneventful. There is a distortion of the frontal structure as the packet approaches the end of the slope (t = 14 in Figure 9) when the trough of the first wave becomes flat.

3.2.5. Deeper Pycnocline

[22] After leaving the bank, the depression almost disappears, as the leading edge moves forward at considerable speed. However, the amplitude of the disturbance is large enough that it eventually steepens under the effect of nonlinearity and evolves into an undular bore, albeit with fewer undulations. The shoaling is very similar to the one observed with standard stratification.

3.3. Simulated Time Series

[23] To facilitate the comparison with observational data, we selected four locations along the slope and outer shelf (named S1-4 in Figure 6) and created virtual time series of temperature from the model output, under standard conditions. The four stations are 1 km apart, yet only at S1 and S2 do the time series resemble each other, showcasing the fact that reconstructing the physical process of NLIWs shoaling from a single station, can be very difficult. At S4 (depth 60 m), the incoming undular bore has not yet felt the bottom. Thus the time series shows a well developed set of high-frequency oscillations, with a definite mode-1 structure. The amplitude of the temperature fluctuations decreases with depth, and near the bottom the temperature hardly departs from its equilibrium. At S3, 1 km inshore and only 8.5 m shallower, the temperature record is markedly different. The mode-1 oscillations, which at S4 made up the high-frequency part of the NLIW train, are now confined to the upper section of the water column, and are significantly distorted. In fact, the water column can be divided in two sections by an interface that deepens with time. Above the interface (dashed line in Figure 10-S3), we still find high-frequency oscillations, albeit with a significant amount of distortion relative to S1. Below, the signal is much noisier, due to shear-induced instabilities. Note how the near bottom temperature increases several degrees, and the occurrence of a shock (at t = 14.5 at S3) abruptly restoring the near bottom temperature.

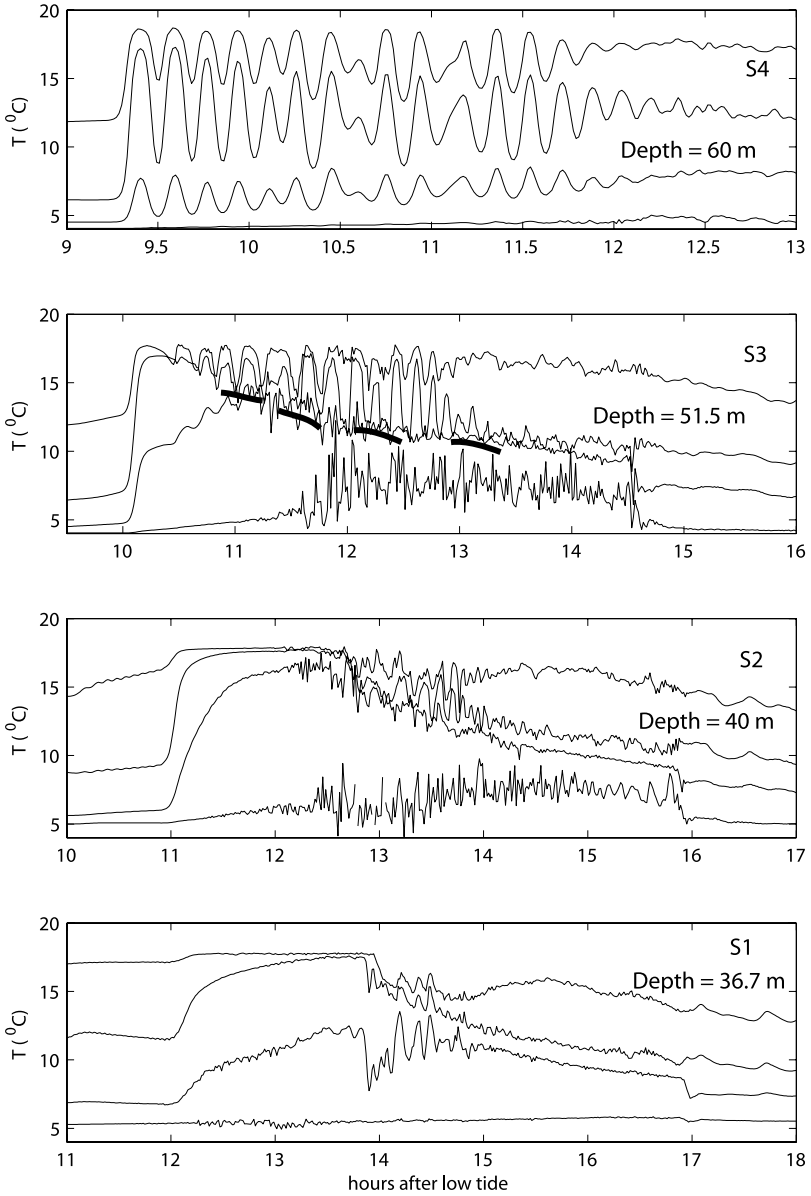

Figure 10. Modeled temperature time series at four stations S1–S4 (Figure 6) along the shoaling slope under standard conditions. At each location we show the temperature at the bottom and at three depths equally spaced straddling the water column. Despite the proximity of the stations, the shoaling undular bore produces markedly different time series. Note the strong resemblance between the time series at S1 and S2 and the time series shown in Figure 3.

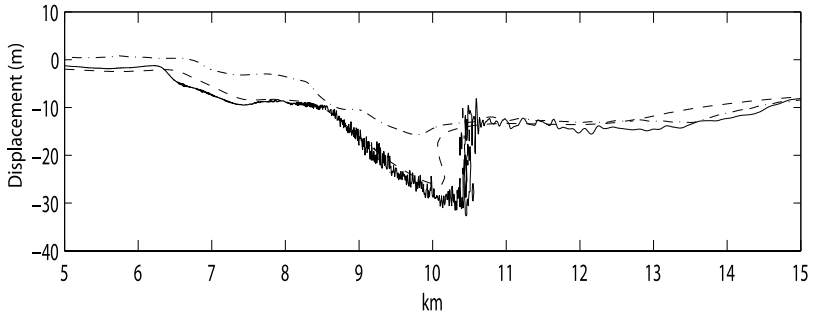

Figure 11. Interface displacement during the shoaling process. Full model (solid line), hydrostatic limit (dashed line) and dispersive limit (dash dotted line).

[24] At S2, the temperature record is qualitatively more similar to the observed time series. The drop in pycnocline depth is more gradual, and very little remains of the coherent high-frequency oscillations of the incoming train. High-frequency "noise" appears after t = 12.5, and again there is a shock restoring stratification near the bottom. At S1, the simulated time series resemble well the temperature record shown in Figure 3d. The displacement of the thermocline is gradual, and with an undular bore partially restoring the stratification after 2 h from the passage of the leading edge. The record at S1 is similar to observations further inshore on the shelf (Figure 18c).

[25] With the aid of these time series we can explain the variability of the observational record. In the field, the exact location where a train of NLIWs will commence shoaling will change from day to day in response to variations in stratification, amplitude of the incoming waves and other factors. As a consequence, the sensors attached to a fixed mooring will "see" different stages of the shoaling, as dictated by the position of the mooring relative to where the train begins to shoal.

[26] Our simulations show that BCEs are complex phenomena, whose details are quite sensitive to specific conditions. Thus we cannot and should not expect a strong quantitative agreement between model and observations.

3.4. Relative Contribution of Dispersion and Nonlinearity

[27] The model can be run with dispersion or nonlinearity turned off. In SBB1 this feature was used to show that during the generation process nonlinearity plays a dominant role. Without dispersion, the disturbance propagates as a bore in the middle of the basin. The effect of dispersion is to generate the series of high-frequency oscillations trailing the leading edge of the bore. Nonetheless, amplitude and position of the envelope were well represented in the nondispersive limit during the propagation in the middle of the basin. We have repeated a similar analysis during shoaling (Figure 11). The full model and the nondispersive model give essentially the same result concerning the distortion of the leading edge of the undular bore. We also obtain good quantitative agreement between the nondispersive model and observations (Figure 12) regarding the magnitude and orientation of the current across the water column during BCEs. The model correctly represents the shift from offshore to onshore as a function of depth.

3.5. Theoretical Models

[28] The shoaling of internal solitary waves in the weakly nonlinear limit has been treated theoretically within the KdV framework [see, e.g., *Grimshaw et al.*, 1999] using as starting point the modified Korteweg-de Vries equation [*Grimshaw et al.*, 1997]. The case at hand is different from the one treated by *Grimshaw et al.* [1999] because the coefficient of the quadratic term in the KdV equation never vanishes along the slope, where model and observations both show NLIWs shoaling, and vanishes on the upper shelf only for the deepest pycnocline considered.

[29] The good agreement between the model in the nondispersive limit and the full model in describing the

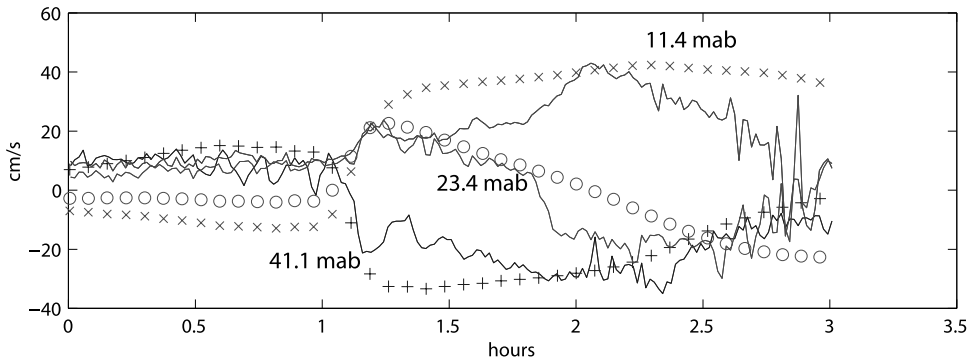

Figure 12. Measured currents at C (solid lines) and currents calculated with the nondispersive model (symbols) during the event are shown in Figure 3b. Time is referenced to an arbitrary reference time.

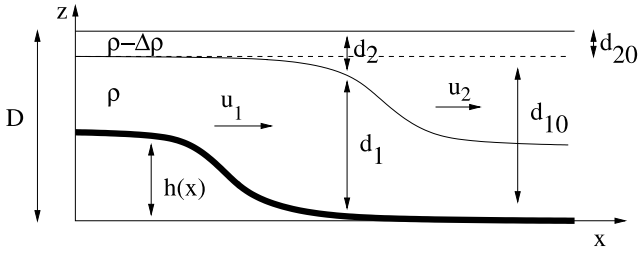

Figure 13. Notation used for the two-layer model. $d_{10,20}$ are the undisturbed depths away from the topography. $d_{1,2}$ the actual depths and $u_{1,2}$ the depth integrated velocities. The displacement is defined as $\eta = d_{20} - d_2 = d_1 - (d_{10} - h)$.

forward section of the shoaling bore suggests that when the waves are large, nonlinearity is the key parameter during shoaling. Thus we consider the same 2-layer fully nonlinear but hydrostatic model that was used in SBB1 to study the generation process. This approach has been used in the past [*Sandstrom and Elliot*, 1984], and more recently employed by *Ostrovsky and Grue* [2003] as an ingredient to derive approximate equations for the evolution of strongly nonlinear internal waves. In the work of *Ostrovsky and Grue* [2003], the focus was on modeling the propagation in uniform depth channels, whereas here we use the two-layer model to diagnose the effect of the shoaling bottom.

[30] If we denote by η the interface displacement and by $v = u_1 - u_2$ the baroclinic velocity (see Figure 13), we have

$$\frac{\partial \eta}{\partial t} + \frac{\partial}{\partial x}\left[\frac{d_2(d_1 v - Q)}{D-h}\right] = 0,$$
$$\frac{\partial v}{\partial t} + \frac{\partial}{\partial x}\left[g'\eta + \frac{(d_2 - d_1)v^2 + 2Qv}{D-h}\right] = 0, \qquad (2)$$

where Q is the barotropic, time-dependent flow rate, $g' = g\Delta\rho/\rho$ the reduced gravity and d_1 and d_2 the thickness of the lower and upper layer respectively [*Baines*, 1995, Chapter 3]. As long as $-1 \leq v/\sqrt{g'(D-h)} \leq 1$, the system above is hyperbolic and can be recast in characteristics form

$$\frac{\partial R^{\pm}}{\partial t} + c^{\pm}(R^+, R^-)\frac{\partial R^{\pm}}{\partial x} = S^{\pm}\frac{\partial h}{\partial x}, \qquad (3)$$

where the speed along characteristics is given by

$$c^{\pm}(R^+, R^-) = \frac{Q}{D-h} + \frac{v(d_2 - d_1)}{D-h} \pm \sqrt{\left(g' - \frac{v^2}{D-h}\right)\left(\frac{d_2 d_1}{D-h}\right)}, \qquad (4)$$

v, d_1, d_2 and $S^{\pm}$ are function of $R^{\pm}$ (the exact functional relationship is given in Appendix A).

[31] To understand the physical mechanism underlying the shoaling process, let us consider a bore-like disturbance given by

$$\eta = \frac{\eta_0}{2}\left(1 + \tanh\frac{x + Vt}{\Delta}\right),$$
$$v = \frac{D-h}{(d_{20} - \eta)(d_{10} - h + \eta)} V\eta, \qquad (5)$$

where V is its leftward (westward in our coordinate system) propagation speed and Δ its characteristic wavelength, moving in an idealized basin whose depth is given by

$$h(x) = D\frac{\alpha}{2}\left(1 - \tanh\frac{x - x_0}{L}\right), \qquad (6)$$

that is a basin bounded to the west by a slope terminating in a plateau. In equations (5) and (6), amplitude and geometric parameters of the bottom are chosen to mimic undular bores approaching the slope-shelf area west of Stellwagen Basin. Furthermore, we assume that the slope of shoaling area $\partial h/\partial x$ is much smaller that the slope of the isopycnals $\partial\eta/\partial x$ (in Massachusetts Bay the former is $O(0.5^\circ)$, whereas the latter is $O(10^\circ)$), so that we can neglect to first order the r.h.s. of equation (3), and $R^{\pm}$ remain constant during the shoaling. Also, the initial condition is such that the right going invariants R^+ emanating from upstream (relative to the direction of propagation of the wave) have constant (zero) value, and finally we set the barotropic transport $Q = 0$. With these assumptions, the left going characteristics over the rise have constant slope. In Figure 14a, we show such a bore at two different locations in the basin. As long as the disturbance remains in the basin, the speed of the leftward going characteristics is larger on the trailing edge relative to the leading edge (Figure 14b), provided $d_2 < d_1$, and dispersion is required to balance nonlinearity. As the wave progresses past the point where d_2 at the trailing edge is larger than d_1, the characteristic with the largest westward velocity shifts from the trailing edge to a point upstream of it, due to the combined effect of the baroclinic self advection (second term in equation (4)) which becomes positive, and the nonlinear wave speed (third term in equation (4)) having a maximum at $d_1 = d_2$. This can be seen in Figure 14b. Hence starting from the trailing edge and spreading forward as the wave keeps moving, nonlinearity flattens the slope of the wave, eventually leading to the formation of a rarefaction wave propagating upslope. Conversely, downstream of the minimum in speed, nonlinearity will tend to steepen whatever disturbance is traveling leftward, leading to the formation of an upslope surge, precisely as we have observed in our numerical experiments (note that the baroclinic advection can dominate the buoyancy response, which would force the trailing edge to move downslope). To make this point clearer, we present the evolution of a single solitary wave (with realistic environmental parameters) approaching the slope using equation (2), assuming the Riemann invariants to be constant along characteristics lines (that is, we neglect the influence of changes in the bottom depth, which is justified for short times if Δ, the scale of the wave, is much smaller than L, the scale of the topography) (Figure 15). The initial sech^2 pulse evolves as explained above, with the leading side becoming aligned with the bottom, and the trailing side steepening. The baroclinic self-advection gives a significant contribution, and the velocity in the lower layer approaches or exceeds the speed of propagation of the wave. We have also compared the evolution of the same pulse using the standard KdV equation, as well as the modified KdV equation [*Grimshaw et al.*, 1997], neglecting in both cases the dispersive terms. The goal is to see how well the

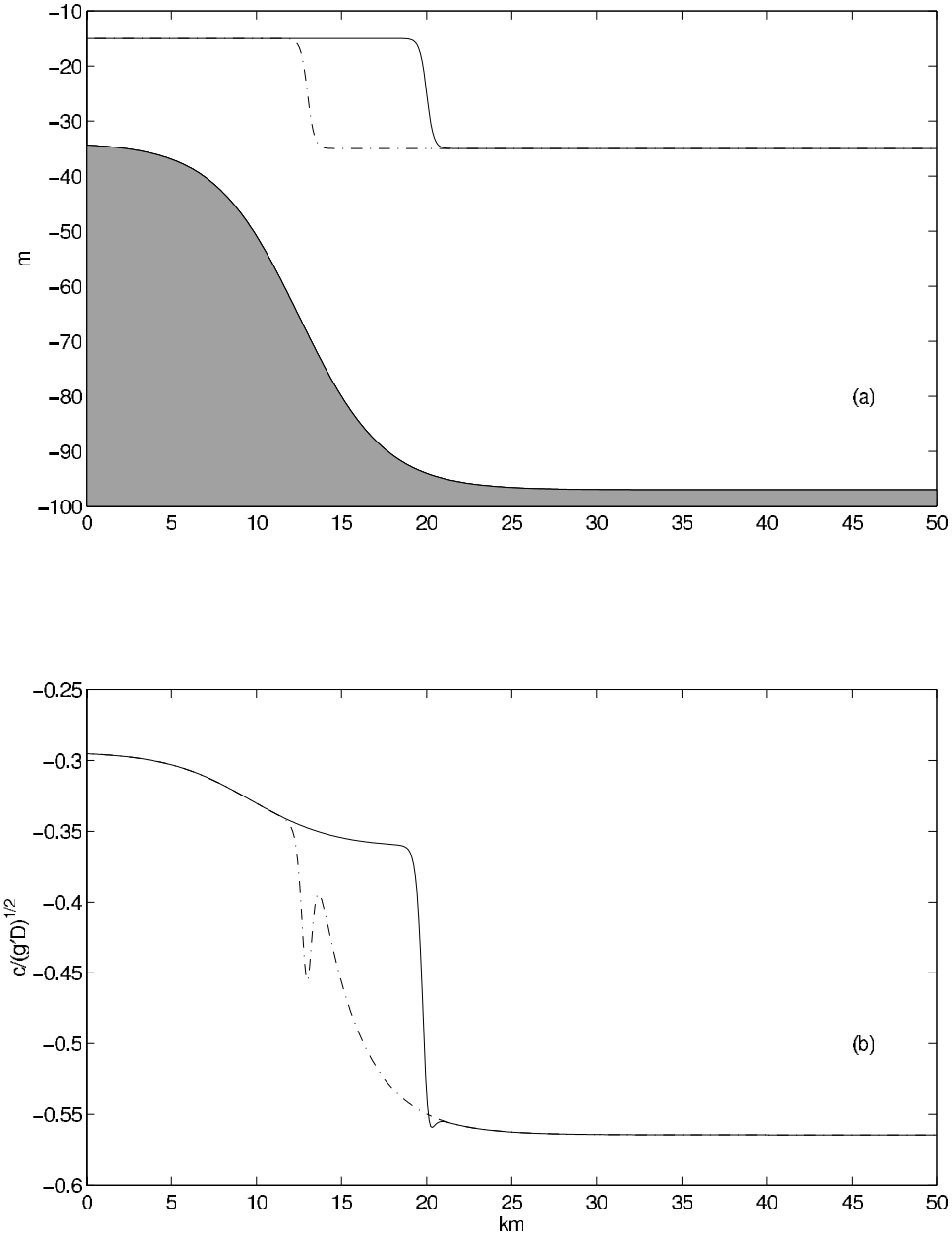

Figure 14. Idealized two-layer model. (a) Isopycnal displacement given by equation bore at two locations in the basin with $\eta_0 = -20$ m, $d_{10} = 82$ m and $\Delta = 400$ m. The profile of the bottom was obtained with $D = 97$ m, $\alpha = 0.65$ and $x_0 = 12.5$ km. (b) The corresponding nonlinear speed of the leftward going characteristics.

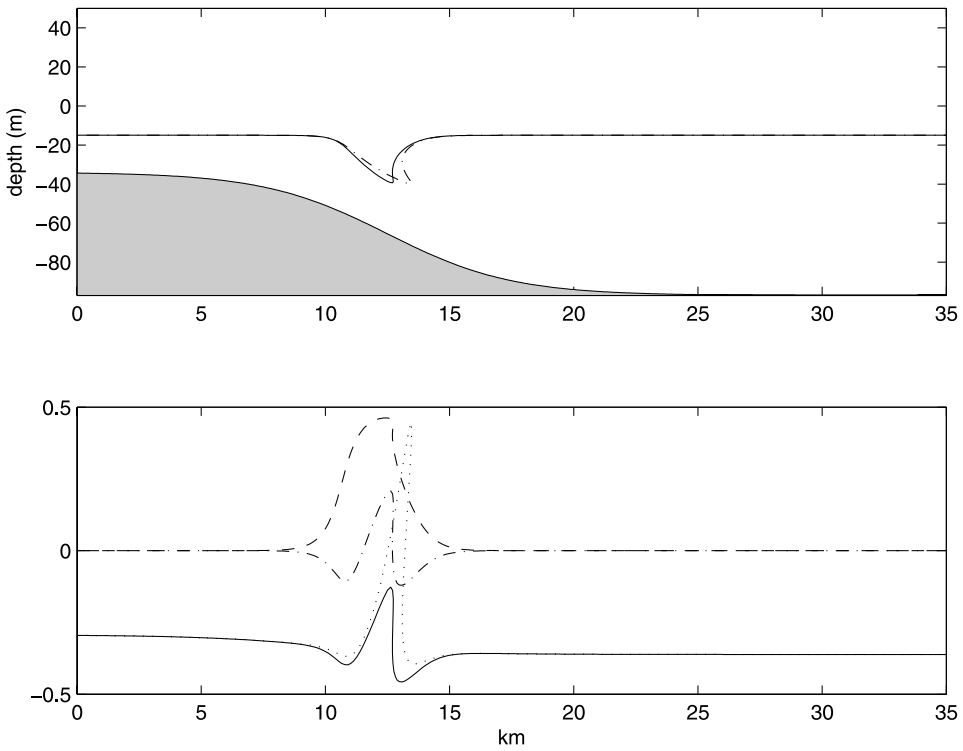

Figure 15. Two-layer, hydrostatic idealization of a single pulse solitary wave propagating into a shoaling area, just before the trailing slope overturns. (top) The displacement of the pycnocline, showing the leading slope becoming parallel to the bottom, and the trailing slope approaching the overturning limit. For comparison, we have also plotted the solution using the "hydrostatic" version of the modified KdV equation (dash-dotted line). (bottom) The speed of the characteristics using the two-layer model (solid line) and using the modified KdV equation (dotted), baroclinic advection (dash dotted line) and velocity in the lower layer (dashed line). The initial shape of the wave was given by $\eta = \eta_0\ \mathrm{sech}^2((\mathrm{x} - \mathrm{x}_0)/\Delta)$, with $\Delta = 1$ km, $x_0 = 13$ km, $\eta_0 = -25$ m, propagating to the left with a speed equal to $0.43\ \sqrt{g'D}$. Environmental parameters as in Figure 14.

hyperbolic character of the system is captured in both cases. Note that since both the *Choi and Camassa* [1999] equation, as well as the beta model derived by *Ostrovsky and Grue* [2003], in the nondispersive limit are equivalent to the two-layer model employed here, we are in effect comparing strongly nonlinear models versus weakly nonlinear models. Looking at the characteristics in space-time (Figure 16), the regular KdV equation does not exhibit the pattern of a shoaling pulse, while the modified KdV equation tends to overestimate the effect of the bottom. Both the 2-layer hydrostatic model and the modified KdV equation show the development of the rarefaction wave along the upslope, followed by the formation of the shock (where characteristics lines intersects). In the modified KdV equation, the shock develops much earlier due to the existence of characteristics that propagate to the east even before the wave approaches the shoaling area. In contrast, the characteristics of the regular KdV equation do not show any rarefaction wave along the slope.

[32] Having established that for large NLIWs nonlinearity controls the process during shoaling, we can use the results above to propose a definition of shoaling and a simple criterion for the onset of shoaling, based on the hyperbolic part of the problem (i.e., neglecting dispersion).

[33] The shoaling process begins when the characteristic with the largest forward velocity shifts from the trough, creating an area forward of the trough where a wave of rarefaction develops. For a two-layer setup, based on this definition, shoaling begins when the trough of the first pulse becomes closer to the bottom than to the surface. The local barotropic tide can have an impact on the location as well. As long as the distance between leading and trailing edge Δ remains small relative to the topographic horizontal length scale L, the effects of the barotropic component Q are small. However, as leading and trailing edge grow farther apart, the change in Q due to the topography can become important. Indeed, if the shoaling happens during ebb tide, the trailing edge is further delayed relative to the leading edge, while the opposite is true if the shoaling process happens during flood.

4. Inshore Evolution

[34] *Scotti and Pineda* [2004] hypothesized that the strongly nonlinear waves of elevation observed near the

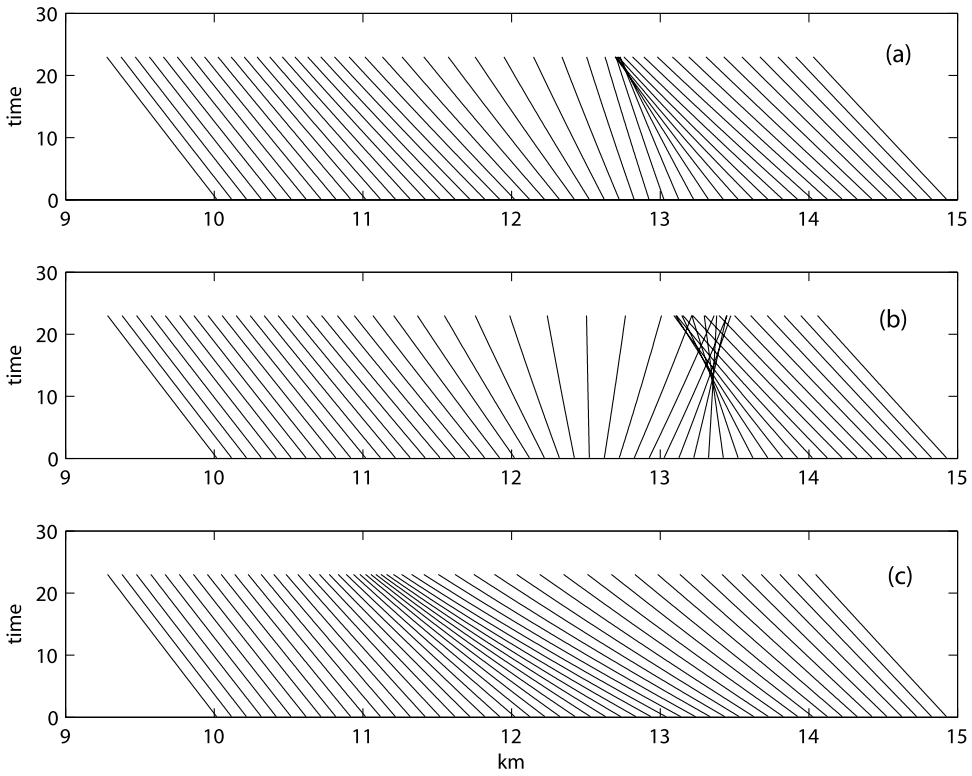

Figure 16. Characteristics emanating from the initial solitary wave. (a) two-layer hydrostatic model. (b) Modified KdV. (c) Regular KdV. Environmental parameters as in Figure 14.

25-m isobath resulted from the evolution of waves of depression observed further offshore. The conjecture was supported by the arrival timing, but lacked a mechanistic explanation, which the above discussion now provides. Even though the 25-m isobath is too close to the boundary in our model to provide reliable quantitative estimates, we can nonetheless extrapolate the results, using the theory developed above. On the shallow ''shelf'' area, we can expect three types of NLIWs (a–c below), depending on the properties of the undular bore approaching from the Stellwagen basin. If (a) the combination of amplitude and pycnocline depth is such that the approaching undular bore does not exceed the critical threshold, we expect that the undular bore will continue unaltered, save for an adiabatic compression of the horizontal scale of the waves (or else the physics becomes hydrostatic). If the amplitude exceeds the critical value, then the incoming undular bore will undergo the transformation outlined in the previous sections. The final product on the shelf depends on the relative depth of the undisturbed pycnocline on the shelf, which determines whether the leading rarefaction wave generated during the shoaling process will remain such, or eventually steepens into a bore. For the latter to occur, the trailing edge of the rarefaction wave has to move faster than the leading edge, and this occurs, e.g., if the undisturbed pycnocline ahead of the wave is close to middepth. In this case, (b) a ''triangular'' internal tide (Figure 17) is expected to develop. Otherwise, (c) a ''square'' internal tide will develop with high-frequency oscillations developing on either end. Examination of the temperature record obtained in September 2001 at the 25-m isobath (location D, Figure 1) shows

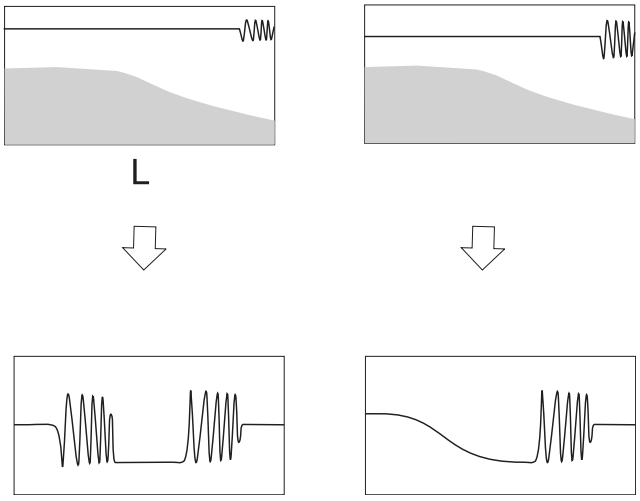

Figure 17. Sketch of possible outcomes of the shoaling process. On the left, the undisturbed pycnocline on the shelf is located above middepth and the leading rarefaction wave develops into an undular bore. This is an example of square tide. On the right, the pycnocline is located at middpeth on the shelf, and the rarefaction wave propagates undisturbed. We refer to this case as a triangular internal tide. In both cases, the pycnocline is restored by an undular bore of elevation.

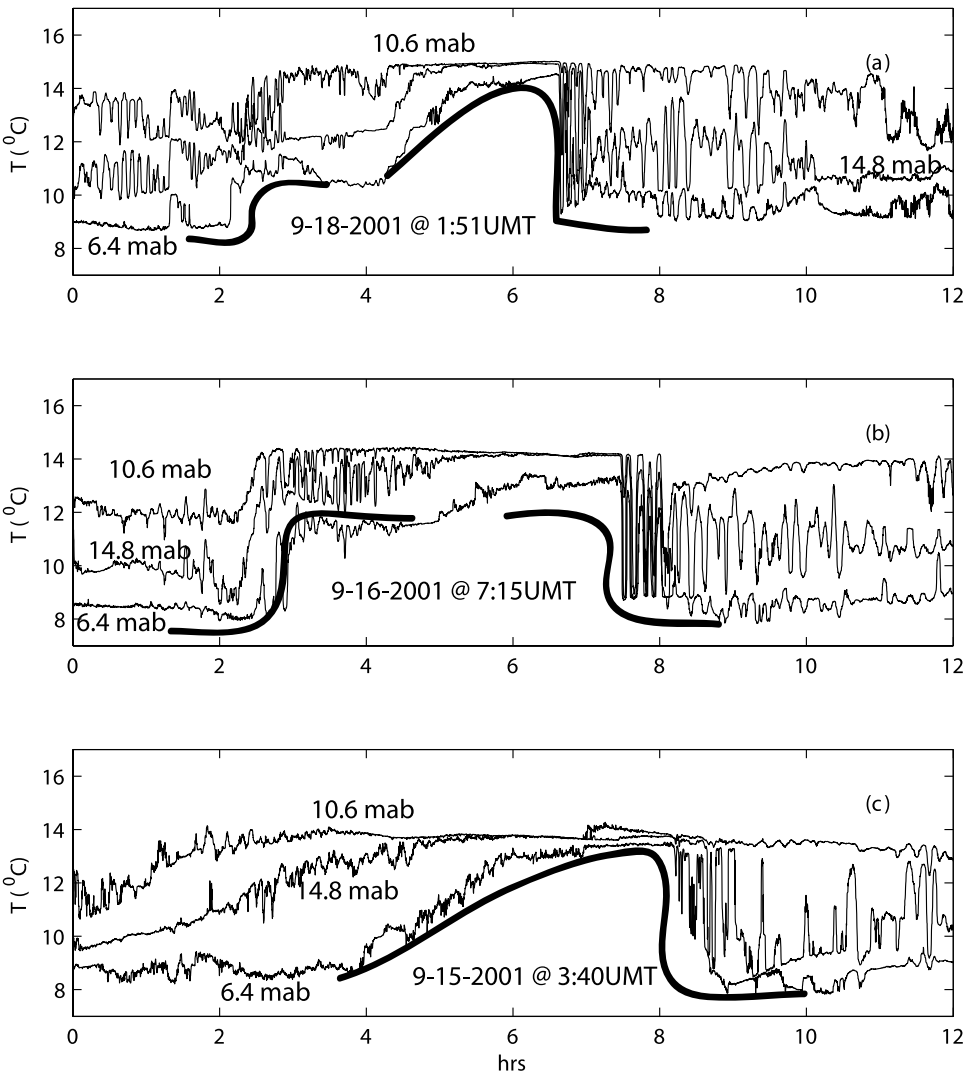

Figure 18. Sample of different types of internal tide envelopes observed at the 25-m isobath in September 2001 (location D in Figure 1). (a) Mixed square-triangular internal tide, (b) square internal tide, and (c) triangular internal tide. The thick lines highlight the underlying envelope of the internal tide. The depth of the instruments is given indicated next to each time series in meters above bottom (mab).

examples of all cases (Figure 18), including one in which a triangular tide is evolving into a square one (Figure 18a).

5. Discussion

[35] In this paper we have studied the process of shoaling of NLIWs in Massachusetts Bay with the aid of a fully nonlinear and nonhydrostatic model. Background stratification and forcing were set to match the conditions observed in the area during the MBIWE98 experiment. The results were compared with the observed density and current observations and found in good agreement. When the undisturbed pycnocline is shallower than 10 m, between the 45- and 50-m isobaths the observations show the passage of nonlinear internal bores with properties similar to the ones observed further offshore. When the pycnocline deepens below 10 m, instead of observing undular bores, we measured very energetic events, whose onset coincided with the expected arrival time of the undular bore that was still observed in the deeper section of the basin. With the help of the model, we were able to show that these events were the manifestation of the strongly nonlinear interaction of the approaching undular bore with the shoaling bottom. The model shows that when the pycnocline is displaced past the local midlevel depth by the leading wave, the undular bore cannot propagate, and this results in a reorganization of the internal wave envelope. Only a fraction of the energy of the NLIWs is lost to mixing during this process. The rest propagates further inshore in the form of a nonlinear internal tide, which can support high-frequency NLIWs, both on its leading as well as on its trailing edge. All of the waveforms predicted by the model were observed at the 25-m isobath. Analysis of virtual time series of temperature generated from the model output show that measured properties of shoaling NLIWs at discrete locations are

highly variable, depending on the location of the mooring relative to the isobath where shoaling begins.

[36] The shoaling process is only marginally affected by dispersion, similarly to what was reported for the generation (SBB1). For this reason, a simple two-layer fully nonlinear but hydrostatic model can be used to diagnose the physics. We have also diagnosed the process with the aid of the original KdV equation, as well as the extended KdV equation. While the former does not capture, even qualitatively, the behavior observed, the latter agrees qualitatively, though quantitatively will tend to misplace the location where the transition takes place. The interaction process also compares well with previous laboratory experiments [*Kao et al.*, 1985], as well as the idealized numerical experiments of *Vlasenko and Hutter* [2002]. However, it differs from the experiments of *Venayagamoorthy and Fringer* [2006] and the modeling work of *Bourgault et al.* [2007] in that no boluses are seen propagating upslope. Likely, the main difference is that in Massachusetts Bay the pycnocline does not intersect the bottom until very close to shore (near the 15-m isobath), a situation also observed in Southern California [*Pineda and Lopez*, 2002] and the Pacific coast of Panama (Pineda, personal observation). Our explanation of the process observed in Massachusetts Bay relies on the fact that waves can still propagate onshore of the shoaling area. Where this is not possible, then boluses are to be expected. However, *Scotti and Pineda* [2004] did find evidence of trapped cores within the high-frequency component of the internal tide packet, in two of the 14 wave trains observed. Whether these are boluses *a la Venayagamoorthy and Fringer* or simply very large high-frequency solitary waves remains to be explained. Perhaps we need to recognize that a nonlinear internal tide is a complex object, which can contain a host of different high-frequency phenomena within its envelope. The focus of this paper has been mostly on the large-scale picture, that is how the nonlinear internal tide as a whole interacts with the shoaling bottom. Better models (with higher resolution), together with further experiments and observations, are needed to clarify all the possible pathways of shoaling for a given set of environmental conditions.

[37] Finally, since the shoaling process induces strong near-bottom offshore currents just above the seafloor, it may explain the abrupt change in bottom texture observed near the 45-m isobath [*Butman et al.*, 2006], where in a very short cross-shore distance compacted gravel leads to sand and silt. This change in texture is reflected in a sharp decrease in backscatter intensity measured as part of multibeam sonar surveys. A similar sharp change in surficial conditions in the cross-shore direction was reported by *Noble and Xu* [2003] in Santa Monica Bay. As in the case discussed here, the pattern was attributed to the passage of internal bores with a structure very similar to the one observed inshore of C in Massachusetts Bay. Of course, there are alternative explanations for the sharp change, based on the subsurface geology, or some geological event in the past. For example, during the last glacial period, there was a low stand of sea level at about 45 m [*Oldale et al.*, 1993]. Thus the area has been reworked twice by advancing sea level [*Knebel and Circe*, 1995]. Thus further research is needed to confirm the link between sharp changes in surficial texture and shoaling NLIWs. Were this link to be confirmed, regions of sharp transition in backscatter intensity may help to identify where NLIWs shoaling undergo BCEs.

Appendix A: Riemann Invariants of the Two-Layer Hydrostatic Model

[38] The Riemann invariants of the two-layer model can be written as

$$R^{\pm} = F \pm G, \tag{A1}$$

where

$$F = \int_0^{\eta} \frac{d\eta}{\sqrt{d_1 d_2}}, \; G = \int_0^{v} \frac{dv}{\sqrt{g'(D-h) - v^2}}, \tag{A2}$$

where $d_1 = d_{10} + \eta - h$ and $d_2 = d_{20} - \eta$ (see Figure 13). The source term is given by

$$S^{\pm} = \frac{u_1}{D-h}\left(\sqrt{\frac{d_2}{d_1}} \mp \frac{v}{\sqrt{g'(D-h) - v^2}}\right) + c^{\pm}\frac{\partial R^{\pm}}{\partial h} \tag{A3}$$

[39] **Acknowledgments.** A. Scotti began this project as a Postdoctoral Scholar at the Woods Hole Oceanographic Institution, with support from the Johnson Foundation and the USGS. Further support was provided to Scotti by the Office of Naval Research under grants N00014-01-1-0172, N00014-03-1-0553, and N00014-05-1-0361, and by NSF under grant OCE 07-29636. R. Beardsley was supported by ONR under grants N00014-98-1-0059, N00014-00-1-0210, and the Smith Chair in Coastal Physical Oceanography. J. Pineda was supported by ONR under grants N00014-01-1-0172, and by a WHOI Ocean Life Institute Fellowship. The authors wish to thank R. Grimshaw, K. Helfrich and M. Noble for useful comments.

References

Apel, J. R. (2003), A new analytical model for internal solitons in the oceans, *J. Phys. Oceanogr.*, *33*, 2247–2269.

Apel, J. R., L. A. Ostrovsky, and Y. A. Stepanyants (1995), Internal solitons in the ocean, *Tech. Rep. MERCJRA0695*, Appl. Phys. Lab., JHU, Baltimore, Md.

Apel, J. R., L. A. Ostrovsky, Y. A. Stepanyants, and J. F. Lynch (2007), Internal solitons in the ocean and their effect on underwater sound, *J. Acoust. Soc. Am.*, *121*, 695–722.

Baines, P. G. (1995), *Topographic Effects in Stratified Flows*, Monogr. on Mech., Cambridge.

Bourgault, D., M. D. Blokhina, R. Mirshak, and D. E. Kelley (2007), Evolution of a shoaling internal solitary wavetrain, *Geophys. Res. Lett.*, *34*, L03601, doi:10.1029/2006GL028462.

Butman, B., P. S. Alexander, S. P. Anderson, F. L. Lightsom, A. Scotti, and R. C. Beardsley (2004a), The Massachusetts Bay internal wave experiment, August 1998: Data report, *Tech. Rep. U. S. Geological Survey Data Series 85*, Washington, D. C. (Available at http://pubs.usgs.gov/ds/2006/85/)

Butman, B., P. C. Valentine, W. W. Danforth, L. Hayes, L. A. Serrett, and T. J. Middleton (2004b), Shaded relief, backscatter intensity and sea floor topography of Massachusetts Bay and the Stellwagen Bank Region, offshore of Boston, Massachusetts, U.S. Geological Survey Geologic Investigation Map I-2734, scale 1:125,000, 2 sheets. U.S. Geol. Surv., Washington, D. C. (Available at http://pubs.usgs.gov/imap/i2734)

Butman, B., P. S. Alexander, A. Scotti, R. C. Beardsley, and S. Anderson (2006), Large internal waves in Massachusetts Bay transport sediments offshore, *Cont. Shelf Res.*, *26*, 2029–2049.

Choi, W., and R. Camassa (1999), Fully nonlinear internal waves in a two-fluid system, *J. Fluid Mech.*, *396*, 1.

Dauxois, T., and W. R. Young (1999), Near-critical reflection of internal waves, *J. Fluid Mech.*, *390*, 271–295.

Grimshaw, R., E. Pelinovsky, and T. Talipova (1997), The modified Korteweg-de Vries equation in the theory of large-amplitude internal waves, *Nonlinear Processes Geophys.*, *4*, 237–250.

Grimshaw, R., E. Pelinovsky, and T. Talipova (1999), Solitary wave transformation in a medium with sign-variable quadratic nonlinearity and cubic nonlinearity, *Physica D*, *132*, 40–62.

Helfrich, K. R. (1992), Internal solitary wave breaking and run-up on a uniform slope, *J. Fluid Mech.*, *243*, 133–154.

Helfrich, K. R., and W. K. Melville (1986), On long non-linear internal waves over slope-shelf, *J. Fluid Mech.*, *167*, 285.

Helfrich, K. R., and W. K. Melville (2006), Long nonlinear internal waves, *Ann. Rev. Fluid Mech.*, *38*, 395–425.

Jackson, C. R. (2004), *An Atlas of Internal Solitary-like Internal Waves*, Global Ocean Assoc., Alexandria, Va. (Available at http://www.internalwaveatlas.com)

Kao, T. W., F.-S. Pan, and D. Renouard (1985), Internal solitons on the pycnocline: Generation, propagation, and shoaling and breaking over a slope, *J. Fluid Mech.*, *159*, 19–53.

Klymak, J. M., and J. N. Moum (2003), Internal solitary waves of elevation advancing on a shoaling shelf, *Geophys. Res. Lett.*, *30*(20), 2045, doi:10.1029/2003GL017706.

Knebel, H. J., and R. C. Circe (1995), Seafloor environments within the Boston Harbor-Massachusetts Bay sedimentary system: A regional synthesis, *J. Coastal Res.*, *11*, 230–251.

Legg, S., and A. Adcroft (2003), Internal wave breaking at concave and convex continental slopes, *J. Phys. Oceanogr.*, *33*, 2224–2246.

Liu, A. K., Y. S. Chang, M.-K. Hsu, and N. K. Liang (1998), Evolution of nonlinear internal waves in the East and South China Seas, *J. Geophys. Res.*, *103*, 7995–8008.

Noble, M. A., and J. P. Xu (2003), Observations of large-amplitude cross-shore internal bores near the shelf break, Santa Monica Bay, CA, *Mar. Environ. Res.*, *56*, 127–149.

Oldale, R. N., S. M. Colman, and G. A. Jones (1993), Radiocarbon ages from two submerged strandline features in the western Gulf of Maine and sea-level curve for the northeastern Massachusetts coastal region, *Quat. Res.*, *40*, 38–45.

Ostrovsky, L. A., and J. Grue (2003), Evolution equations for strongly nonlinear internal waves, *Phys. Fluids*, *15*, 2934–2948.

Pineda, J., and M. Lopez (2002), Temperature, stratification and barnacle larval settlement in two California sites, *Cont. Shelf Res.*, *22*, 1183–1198.

Ramp, S. R., T. Y. Tang, T. F. Duda, J. F. Lynch, A. K. Liu, C.-S. Chiu, F. L. Bahr, H.-R. Kim, and Y.-J. Yang (2004), Internal solitons in the northeastern South China Sea. Part I: Sources and deep water propagation, *IEEE J. Oceanic Eng.*, *29*, 1157–1181.

Sandstrom, H., and J. A. Elliot (1984), Internal tide and solitons on the Scotian Shelf, *J. Geophys Res.*, *89*, 6415.

Scotti, A., and J. Pineda (2004), Observation of very large and steep waves of elevation near the Massachusetts coast, *Geophys. Res. Lett.*, *31*, L22307, doi:10.1029/2004GL021052.

Scotti, A., R. C. Beardsley, and B. Butman (2007), Generation and propagation of nonlinear internal waves in Massachusetts Bay, *J. Geophys. Res.*, *112*, C10001, doi:10.1029/2007JC004313.

Stanton, T. P., and L. A. Ostrovsky (1998), Observations of highly nonlinear, tidally forced solitons over the continental shelf, *Geophys. Res. Lett.*, *25*, 2695.

Trask, R. P., and M. G. Briscoe (1983), Detection of Massachusetts Bay internal waves by the synthetic aperture radar (SAR) on SEASAT, *J. Geophys. Res.*, *88*, 1789–1799.

Venayagamoorthy, S. K., and O. B. Fringer (2006), Numerical simulations of the interaction of internal waves with a shelf break, *Phys. Fluids*, *18*, 076603.

Vlasenko, V., and K. Hutter (2002), Numerical experiments of the breaking of solitary internal waves over a slope-shelf topography, *J. Phys. Oceanogr.*, *32*, 1779–1793.

Vlasenko, V., L. Ostrovsky, and K. Hutter (2005a), Adiabatic behavior of strongly nonlinear internal soiltary waves in slope-shelf areas, *J. Geophys. Res.*, *110*, C04006, doi:10.1029/2004JC002705.

Vlasenko, V., N. Stashchuck, and K. Hutter (2005b), *Baroclinic Tides*, Cambridge Univ. Press, New York.

R. C. Beardsley, Department of Physical Oceanography, Woods Hole Oceanographic Institution, MS# 21, Woods Hole, MA 02543, USA. (rbeardsley@whoi.edu)

B. Butman, U.S. Geological Survey, Woods Hole Science Center, 384 Woods Hole Road, Woods Hole, MA 02543–1598, USA. (bbutman@usgs.gov)

J. Pineda, Department of Biology, Woods Hole Oceanographic Institution, MS# 50, Woods Hole, MA 02543, USA. (jpineda@whoi.edu)

A. Scotti, Department of Marine Sciences, University of North Carolina, CB 3300, Chapel Hill, NC 27599–3300, USA. (ascotti@unc.edu)